

Extending the Heat Index

YI-CHUAN LU^{a,b} AND DAVID M. ROMPS^{b,c}

^a *Department of Physics, University of California, Berkeley, California*

^b *Climate and Ecosystem Sciences Division, Lawrence Berkeley National Laboratory, Berkeley, California*

^c *Department of Earth and Planetary Science, University of California, Berkeley, California*

(Manuscript received 17 February 2022, in final form 10 May 2022)

ABSTRACT: The heat index is a widely used measure of apparent temperature that accounts for the effects of humidity using Steadman's model of human thermoregulation. Steadman's model, however, gives unphysical results when the air is too hot and humid or too cold and dry, leading to an undefined heat index. For example, at a relative humidity of 80%, the heat index is only defined for temperatures in the range of 288–304 K (59°–88°F). Here, Steadman's thermoregulation model is extended to define the heat index for all combinations of temperature and humidity, allowing for an assessment of Earth's future habitability. The extended heat index can be mapped onto physiological responses of an idealized human, such as heat exhaustion, heat stroke, and even heat death, providing an indication of regional health outcomes for different degrees of global warming.

SIGNIFICANCE STATEMENT: The existing heat index is well-defined for most combinations of high temperature and humidity experienced on Earth in the preindustrial climate, but global warming is increasingly generating conditions for which the heat index is undefined. Therefore, an extension of the original heat index is needed. When extending the heat index, we use the same physiological model as in the original work of Steadman to ensure backward compatibility. Following Steadman, each value of the heat index is mapped onto a measurable physiological variable, which can be useful for assessing the health impacts of various combinations of temperature and humidity, especially for outdoor workers.

KEYWORDS: Conservation equations; Indices; Nonlinear models; Health

1. Introduction

For a given combination of air temperature and humidity, the heat index is the air temperature at a reference water-vapor pressure of 1.6 kPa that would be experienced in the same way by a human. The heat index is calculated from a model of human thermoregulation assuming optimal physiology (with regard to the core-to-skin blood flow and sweat rate), optimal behavior (with regard to the choice of clothing), and optimal circumstances (in the shade with unlimited water). The heat index thus defined is widely used in the United States to communicate the health risk associated with high heat and humidity.

Despite its utility, the heat index is defined only within certain bounds of temperature and humidity because of some unphysical conditions occurring in the underlying human model when pushed outside those bounds (Steadman 1979). For example, at a relative humidity of 80%, the heat index is not defined for temperatures above 304 K (31°C, or 88°F) or below 288 K (15°C, or 59°F) because the vapor pressure at the skin or in the air becomes supersaturated. These unphysical conditions will be discussed in detail later. To circumvent these problems, polynomial fits are often used to extrapolate the heat index to higher temperatures (Rothfus 1990; Anderson et al. 2013), including by the National Weather Service (2014), but those extrapolations have no basis in science.

In the current climate, the heat index is undefined over large swaths of Earth at any given moment on average, mainly because of cold conditions, but also on occasion because of hot and humid conditions. As an example, Fig. 1 shows the occurrence frequency for each near-surface temperature–humidity combination at the U.S. Department of Energy's Atmospheric Radiation Measurement (ARM) Southern Great Plains (SGP) site (Mather and Voyles 2013) measured every minute during June, July, and August (JJA) from 2012 to 2021, inclusive. The hatched areas are where the existing heat index is undefined. In the current climate, 5% of these 920 SGP summer days have an undefined heat index because of sufficiently cold and dry conditions, but only 0.9% of the summer days have an undefined heat index caused by sufficiently hot and humid conditions. To estimate how often an undefined heat index would occur at a substantially different temperature anomaly (e.g., in a business-as-usual scenario in the twenty-second century), we add 10 K to the JJA temperature while keeping the humidities unchanged. The peak of the distribution shifts out of the defined region, causing 91% of the SGP summer days to have an undefined heat index. Even a more modest +5 K warming (not shown) would cause the heat index to be undefined at some point during 39% of the SGP summer days.

To quantify future conditions using the heat index, it is necessary to extend the existing definition. Previous studies have used the heat index to explore warming scenarios (e.g., Delworth et al. 1999; Diffenbaugh et al. 2007; Opitz-Stapleton et al. 2016; Diem et al. 2017; Modarres et al. 2018; Dahl et al.

Corresponding author: Yi-Chuan Lu, yclu@berkeley.edu

DOI: 10.1175/JAMC-D-22-0021.1

© 2022 American Meteorological Society. For information regarding reuse of this content and general copyright information, consult the [AMS Copyright Policy \(www.ametsoc.org/PUBSReuseLicenses\)](https://www.ametsoc.org/PUBSReuseLicenses).

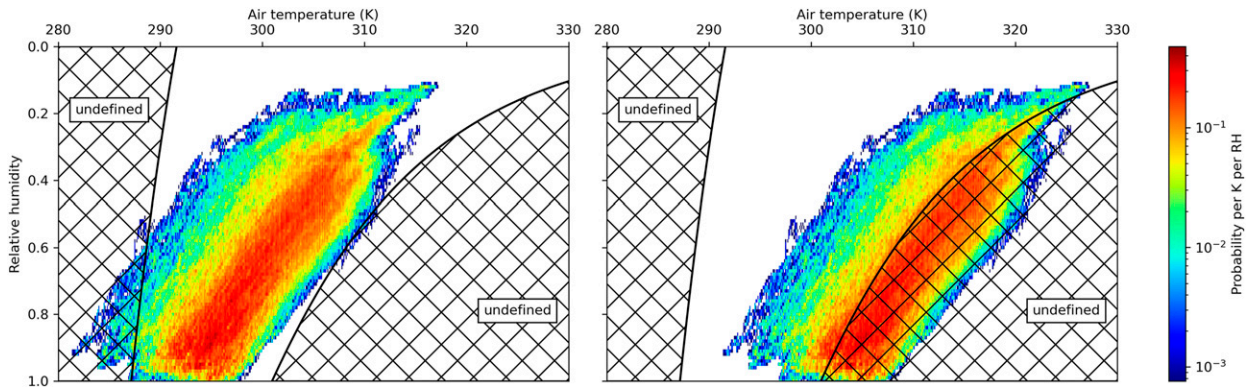


FIG. 1. (left) Joint probability density of near-surface 1-min air temperature and relative humidity at the ARM SGP site during JJA from 2012 to 2021. The hatched regions show where the heat index is undefined. (right) As in the left panel, but translating the density to warmer temperatures by 10 K, representing conditions that could be achieved in the twenty-second century with business-as-usual fossil-fuel burning.

2019; Rao et al. 2020; Rahman et al. 2021; Amnuaylojaroen et al. 2022), but those studies used the aforementioned polynomial extrapolation and, therefore, they have relied on extrapolated values that have no grounding in physiology and no basis for interpretation with regard to health impacts. In this paper, we aim to extend the heat index by correcting the underlying model of thermoregulation.

While several different “apparent” or “equivalent” temperatures have been proposed, we focus on the heat index, as defined by Steadman (1979), because it is widely used and, unlike other apparent temperatures, Steadman’s underlying model of human thermoregulation does not depend on uncertain physiological relations. Instead, Steadman’s model assumes an ideal human and requires only easily measured physical parameters such as body mass, skin area, metabolic rate, and tissue conductance. Because the heat index is so widely used, one of the goals here is to ensure backward compatibility; that is, we wish to extend the heat index to cover all conditions without affecting the heat index values already in use. In so doing, we adopt Steadman’s original approach of assuming optimal behavior, physiology, and circumstances. This assumes a best-case scenario with regard to a human’s physical conditioning and access to water and shade: no limits are placed on the human’s capacity to sweat or pump blood to the skin, it is assumed that the human’s behavior with regard to choice of clothing is optimal, and the human is assumed to be in the shade with unlimited drinking water. For consistency, we use these same ideal assumptions when extending the heat index. Therefore, the thermoregulation model presented here, as with the original, represents an upper limit on the capacity of humans to endure high heat and humidity.

2. Derivation of the heat index

In Steadman’s model of human thermoregulation, the human is modeled as an interior core (with temperature T_c) covered by a combination of exposed skin (with exterior temperature T_s) and clothed skin (with exterior temperature \bar{T}_s), as shown in Fig. 2. The clothed skin occupies a fraction ϕ of the total skin

area and is covered with clothing (with exterior temperature T_f , whose subscript f denotes “fabric”). Each of these components also has its own vapor pressure at its outermost layer, denoted by p_c , p_s , \bar{p}_s , and p_f , where the vapor pressure of the core p_c is understood as the saturation vapor pressure of the saline solution in the human body. The skin, clothing, and boundary layer of air around the human are assumed to be sufficiently thin that their storage (or tendencies) of energy and water can be ignored. (Here and throughout, “boundary layer” refers to the layer of turbulent air in the vicinity of the human’s skin and clothing, not the atmospheric boundary layer between Earth’s surface and free troposphere.) Denoting the air temperature and vapor pressure by T_a and p_a , there are seven equations expressing conservation of energy and water mass:

$$0 = Q - Q_v - \phi \frac{T_c - \bar{T}_s}{R_s} - (1 - \phi) \frac{T_c - T_s}{R_s} \quad \text{(energy of steady-state core),} \quad (1)$$

$$0 = \frac{T_c - T_s}{R_s} - \frac{T_s - T_a}{R_a} - \frac{p_s - p_a}{Z_a} \quad \text{(energy at exterior of exposed skin),} \quad (2)$$

$$0 = \frac{T_c - \bar{T}_s}{R_s} - \frac{\bar{T}_s - T_f}{R_f} - \frac{\bar{p}_s - p_f}{Z_f} \quad \text{(energy at exterior of clothed skin),} \quad (3)$$

$$0 = \frac{\bar{T}_s - T_f}{R_f} - \frac{T_f - T_a}{R_a} \quad \text{(energy at exterior of clothing),} \quad (4)$$

$$0 = \frac{p_c - p_s}{Z_s} - \frac{p_s - p_a}{Z_a} \quad \text{(water at exterior of exposed skin),} \quad (5)$$

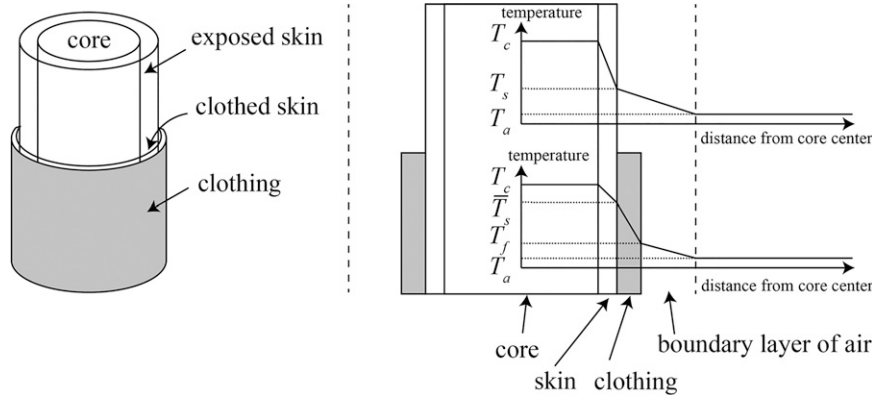


FIG. 2. (left) The geometry of the human model, with the core, exposed skin, clothed skin, and clothing labeled. (right) The cross-sectional view of the human model, with the boundary layer of air drawn explicitly. On top of the cross-sectional view are illustrative temperature distributions along the radial direction of the human model through exposed skin (top axes) and through clothed skin (bottom axes).

$$0 = \frac{p_c - \bar{p}_s}{Z_s} - \frac{\bar{p}_s - p_f}{Z_f} \quad \text{(water at exterior of clothed skin), and} \quad (6)$$

$$0 = \frac{\bar{p}_s - p_f}{Z_f} - \frac{p_f - p_a}{Z_a} \quad \text{(water at exterior of clothing),} \quad (7)$$

where the R and Z variables denote heat transfer resistance and mass transfer resistance, respectively. Specifically, R_s is the resistance to heat flux by the skin (exposed or clothed), R_f is the clothing resistance, R_a is the resistance of the air's boundary layer around the exposed skin, and \bar{R}_a is the resistance of the boundary layer around the clothing. Similar definitions apply to Z_s , Z_f , Z_a , and \bar{Z}_a , which give the resistance to water flux. The convention here is that the overbarred variables are those pertaining to clothing while exposed skin is represented by unbarred quantities. The expressions of R and Z variables are taken from Steadman (1979) (and are summarized in Tables 2–5, described in more detail below), with the exception that the exact T^4 longwave radiation expression is used instead of the linearized equation to account for the full range of air temperatures.

The seven governing equations can be understood as follows. Equation (1) is the equation for conservation of energy in the steady-state core; if we were not assuming steady state, a term proportional to dT_c/dt would appear on the left-hand side. The sources and sinks of energy for the core are the metabolic rate, ventilative cooling, and the transfer of sensible heat from the core to the clothed and unclothed skin. The constant Q is the metabolic rate per skin area, and Q_v is the cooling per skin area within the lungs due to ventilation (i.e., breathing) defined by (Steadman 1979; Fanger 1970):

$$Q_v \equiv \eta Q \left[c_{pa}(T_c - T_a) + \frac{L\hat{R}_a}{\hat{R}_v p} (p_c - p_a) \right], \quad (8)$$

where η is a constant relating metabolic rate to ventilation rate, the constants \hat{R}_a and \hat{R}_v are the specific gas constants of air and vapor (which are given hats to distinguish them from the resistances), c_{pa} is the heat capacity of air at constant pressure, and L is the latent heat of vaporization at the core temperature T_c . Equation (2) expresses the sensible heat budget of the surface of the exposed skin. Because the surface of the skin is a two-dimensional interface, it has no mass and so no tendency term. The skin and boundary layer are thin, so the fluxes can be expressed linearly in terms of temperature or vapor pressure at their interfaces. In this way, the temperature of the exposed skin surface is determined diagnostically, that is, by solving algebraic equations rather than solving differential equations. Note that the exposed skin has three heat sources that must balance at every moment: heat transferred through the skin (by conduction through tissue and transport by blood), heat lost through the air's boundary layer (by conduction and advection), and evaporative cooling of sweat (by diffusion and advection of water vapor through the boundary layer). Equation (3) gives a similar governing equation for clothed skin, except that the clothed skin transfers heat and water vapor through the clothing instead of through the boundary layer. Like the skin, the clothing is treated as having zero heat capacity, so its exterior temperature T_f is set diagnostically by Eq. (4), which states that the rate of sensible heat passing through the clothing (from the exterior of the clothed skin at \bar{T}_s to the exterior of the clothing at T_f) must equal the rate of sensible heat passing through the boundary layer (from the exterior of the clothing at T_f to the ambient air at T_a). Equations (5)–(7) express continuity of mass fluxes at the exterior surfaces of the exposed skin, clothed skin, and clothing, respectively. As will be discussed later, the fabric resistance R_f and Z_f are proportional to the clothing thickness, and the skin resistance R_s and Z_s are related to the skin blood flow, which controls the heat and mass transfer between the core and the skin.

Table 1 defines some of the parameters mentioned above that are used in our extended version of Steadman's model. The

parameters describing the thermodynamic properties of water are optimized to give the best fit of the analytical saturation

vapor pressure to experimental values (Romps 2017). In terms of these constants, the saturation vapor pressure p^* is given by

$$p^*(T) = \begin{cases} p_{\text{trip}} \left(\frac{T}{T_{\text{trip}}} \right)^{(c_{\text{pv}} - c_{\text{vl}})/\hat{R}_v} \exp \left[\frac{E_{0v} - (c_{\text{vv}} - c_{\text{vl}})T_{\text{trip}} \left(\frac{1}{T_{\text{trip}}} - \frac{1}{T} \right)}{\hat{R}_v} \right] & T \geq T_{\text{trip}} \\ p_{\text{trip}} \left(\frac{T}{T_{\text{trip}}} \right)^{(c_{\text{pv}} - c_{\text{vs}})/\hat{R}_v} \exp \left[\frac{E_{0v} + E_{0s} - (c_{\text{vv}} - c_{\text{vs}})T_{\text{trip}} \left(\frac{1}{T_{\text{trip}}} - \frac{1}{T} \right)}{\hat{R}_v} \right] & T < T_{\text{trip}} \end{cases}, \quad (9)$$

which replaces the linearized equation used in Steadman (1979).

Given T_a , p_a , ϕ , the resistances R_s and R_f , and the fact that $p_c = \phi_{\text{salt}} p^*(T_c)$, there are seven unknowns (T_c , T_s , p_s , \bar{T}_s , \bar{p}_s , T_f , and p_f) and seven Eqs. (1)–(7). (As we will see, the variables R_a , \bar{R}_a , Z_a , \bar{Z}_a , Z_s , and Z_f are all functions of some combination of these seven unknowns and/or other specified parameters.) In general, however, solving these seven equations will give a core temperature T_c that is far from the desirable equilibrium value of 310 K. Since human biochemistry functions only when the core temperature is within a narrow range of a few degrees, this is clearly not how the human body works. Instead, the body relies on a combination of behavioral and physiological mechanisms to maintain a stable and standard core temperature. Mathematically, those mechanisms manifest as the introduction of an eighth equation,

$$T_c = 310 \text{ K}, \quad (10)$$

and, to ensure the system is not overdetermined, the conversion of a constant (e.g., R_s or R_f) to a variable. Solving those eight equations in eight unknowns gives not just the temperatures and vapor pressures of the clothing and skin, but also the ideal behavioral or physiological “choice” for the new variable. For example, in very cold conditions, the ideal behavioral response to a change in temperature would be to add or subtract layers of clothing so that the corresponding value of R_f solves the seven original equations plus $T_c = 310 \text{ K}$. Or, in very hot and humid conditions, the ideal physiological response to a change in temperature or humidity would be to change the core-to-skin blood flow so that the corresponding value of R_s gives $T_c = 310 \text{ K}$. In what follows, we will identify the physiological/behavioral adaptations that an ideal human would use in each of six disjoint subsets or “regions” of temperature–humidity pairs spanning temperature–humidity space (i.e., all combinations of temperature and humidity).

The original heat index is defined in what we refer to here as regions III and IV, in which an ideal human chooses to be clothed or naked, respectively. As acknowledged in the original paper (Steadman 1979), Steadman’s model gives unphysical results when the air temperature becomes too cold (at the cold boundary of region III) or too warm (at the hot boundary of region IV). When the air temperature falls below 287–292 K (the precise value depends on the relative humidity), the heat index fails because the reference vapor

pressure of 1.6 kPa exceeds the saturation vapor pressure at the temperature equal to the heat index. When the air temperature rises above 301–350 K (again, depending on the relative humidity), the heat index fails again, this time because the skin’s vapor pressure exceeds its saturation vapor pressure. In the following derivations, we start from region III and extend the heat index from its cold end into the new regions II and I. We then move to region IV and extend the heat index from its warm end into regions V and VI, which are the main focus of this paper.

a. Regions II and III: Clothed

Steadman (1979) gave a simplified schematic of the equations of energy and mass conservation using circuits. The analogy to circuits allows for a visualization of the entire equation set in a compact diagram, so we will present the circuit diagrams for each of the six regions. The most complicated of these circuit diagrams represents region III and is shown in Fig. 3. From top to bottom, the three circuits represent the following: 1) the transfer of water mass through clothed skin and clothing (where “current” is the rate of vapor mass transfer and “potential” is the vapor pressure), 2) the transfer of sensible heat through both clothed and exposed skin (where “current” is the rate of heat transfer and “potential” is the temperature), and 3) the transfer of water mass through exposed skin. As water passes from skin to either the clothing or the air, it evaporates, generating an evaporative cooling that is represented by a controlled current source in the middle circuit. The current (of sensible heat) passing through those controlled current sources is proportional to the respective current (of water mass); this is represented by the vapor pressure terms in Eqs. (2) and (3), which express conservation of energy for the exposed and clothed skin.

In the middle circuit, there is a fixed current source in the core representing the net generation of sensible heat there ($Q - Q_v$). That “current” must pass out to the environment at temperature T_a through some combination of evaporative cooling from the skin (as dictated by the other two circuits) or conduction of sensible heat through either the clothing or exposed skin. The node labeled with temperature T_c is just a point in the circuit and, like a point on a wire in a real electrical circuit, cannot store current. Therefore, Fig. 3 represents the equilibrated solution to Eqs. (1)–(7).

TABLE 1. Constants that are common to all six regions.

| Variable | Value | Interpretation |
|----------------------|--|---|
| T_{trip} | 273.16 K | Triple-point temperature |
| p_{trip} | 611.65 Pa | Triple-point pressure |
| E_{0v} | $2.3740 \times 10^6 \text{ J kg}^{-1}$ | Difference in energy between vapor and liquid at the triple point |
| E_{0s} | $0.3337 \times 10^6 \text{ J kg}^{-1}$ | Difference in energy between liquid and solid at the triple point |
| \hat{R}_a | $287.04 \text{ J kg}^{-1} \text{ K}^{-1}$ | Specific gas constant of air |
| \hat{R}_v | $461 \text{ J kg}^{-1} \text{ K}^{-1}$ | Specific gas constant of vapor |
| c_{va} | $719 \text{ J kg}^{-1} \text{ K}^{-1}$ | Heat capacity of air at constant volume |
| c_{vv} | $1418 \text{ J kg}^{-1} \text{ K}^{-1}$ | Heat capacity of vapor at constant volume |
| c_{vl} | $4119 \text{ J kg}^{-1} \text{ K}^{-1}$ | Heat capacity of liquid at constant volume |
| c_{vs} | $1861 \text{ J kg}^{-1} \text{ K}^{-1}$ | Heat capacity of solid at constant volume |
| c_{pa} | $c_{va} + \hat{R}_a$ | Heat capacity of air at constant pressure |
| c_{pv} | $c_{vv} + \hat{R}_v$ | Heat capacity of vapor at constant pressure |
| L | $E_{0v} + (c_{vv} - c_{vl})(310 \text{ K}) - T_{\text{trip}}$ | Latent enthalpy of evaporation at 310 K |
| p_{a0} | $1.6 \times 10^3 \text{ Pa}$ | Reference vapor pressure for the heat index (Steadman 1979) |
| M_c | 83.6 kg | Mass of the core, taken as the average of the masses of adult men and women in the United States during 2015–16 (Fryar et al. 2018) |
| H | 1.69 m | Height, taken as the average of heights of adult men and women in the United States during 2015–16 (Fryar et al. 2018) |
| A | $(0.202 \text{ m}^2) \left(\frac{M_c}{1 \text{ kg}} \right)^{0.425} \left(\frac{H}{1 \text{ m}} \right)^{0.725}$ | Area of the skin (Parsons 2014) |
| c_{pc} | $3492 \text{ J kg}^{-1} \text{ K}^{-1}$ | Specific heat capacity of the core at constant pressure (Gagge et al. 1972) |
| Q | 180 W m^{-2} | Metabolic rate per skin area for walking (Newburgh 1949; Steadman 1979) |
| ϕ_{salt} | 0.9 | Effective relative humidity of saline solution (Buettner 1959; Steadman 1979) |
| p | $1.013 \times 10^5 \text{ Pa}$ | Air pressure |
| η | $1.43 \times 10^{-6} \text{ kg J}^{-1}$ | Ratio of ventilation rate (kg s^{-1}) to metabolic rate (J s^{-1}) (Fanger 1970) |
| σ | $5.67 \times 10^{-8} \text{ W m}^{-2} \text{ K}^{-4}$ | Stefan–Boltzmann constant |

In this circuit, imagine that the potentials p_a and T_a are given and that we also specify the clothing fraction ϕ and the various resistances. In this case, the values of T_c , T_s , p_s , \bar{T}_s , \bar{p}_s , T_f , and p_f in this circuit (which one could measure in a real electrical circuit with a voltmeter) would be the steady-state solution to Eqs. (1)–(7). For an arbitrarily chosen values of ϕ and the resistances, however, this would likely to give a core temperature T_c that is incompatible with life.

In region III, the fix is to allow the human to choose R_f by wearing an appropriate number and type of clothing layers. By letting R_f be a free variable, we are free to peg the core temperature to the standard value. In other words, the equation set governing the ideal human in region III is Eqs. (1)–(7) and (10), and the variables to be solved for are the original seven plus R_f . The parameters used in region

III are given in Table 2. These are mainly taken directly from Steadman (1979) to maintain backward compatibility of our heat index with the one that has been in use for several decades. Minor modifications have been made, however, to allow the heat index to be extended to a much wider range of temperatures. For example, as mentioned before, the full nonlinear T^4 expression for longwave emission is retained instead of using the linearized expression in Steadman (1979). Appendix A describes how to solve the equations numerically for this region and the others.

In region III, the heat index is the value of T_a that would give the same R_f at the reference vapor pressure of $p_a = p_{a0} \equiv 1.6 \text{ kPa}$. For a T_a that is sufficiently low, p_a will be greater than $p^*(T_a)$, and the heat index becomes unphysical. To extend the heat index to lower temperatures, we define the

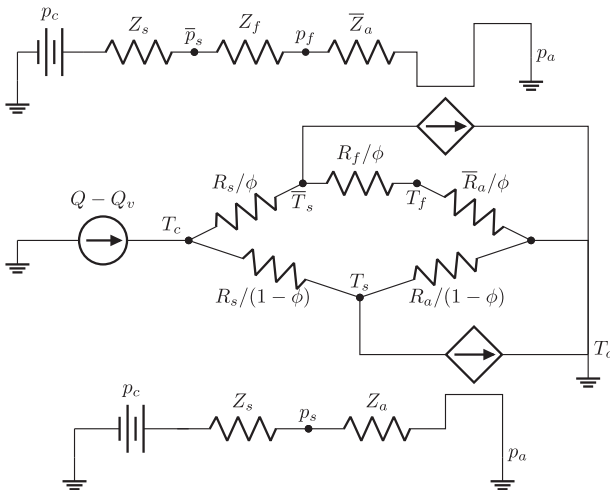


FIG. 3. Diagram illustrating the potentials and resistances for sensible heat transfer (middle circuit) and water transfer (top and bottom circuits), with all three circuits applying to both regions II and III. Region III is one of the two original cases of Steadman (1979). Region II is where we extend the heat index by using $p_a = p^*(T_a)$ instead of $p_a = 1.6$ kPa for the reference vapor pressure. The controlled current sources represent evaporative cooling, which is controlled by the current in the water-transfer circuits. Subscripts $c, s, f,$ and a denote core, skin, fabric, and air, respectively, with temperatures and vapor pressures denoting values at the outermost edges of those components.

reference vapor pressure as $p_a = p^*(T_a)$ in region II. Stated another way, the heat index in regions II and III is the T_a that would give the same R_f with $p_a = \min[p_{a0}, p^*(T_a)]$. Given R_f and the requirement that $p_a = \min[p_{a0}, p^*(T_a)]$, we can solve for T_a by using a root solver to find the T_a that gives, using the procedure above, the correct R_f .

b. Region I: Covering

In conditions that are too cold and dry, we will be unable to find a physical solution in region II. This occurs because the core cannot be maintained at 310 K even with clothing of infinite thickness, that is, with R_f , and thus also Z_f , equal to infinity. In such cold and dry conditions, the fraction ϕ of the skin covered in clothing must be increased above 0.84. Therefore, we define region I as having $R_f = \infty$ and variable $\phi > 0.84$. In this limit, $T_f = T_a, p_f = p_a, \bar{T}_s = T_c, \bar{p}_s = p_c$, and conservation Eqs. (1)–(7) simplify to

$$0 = Q - Q_v - (1 - \phi) \frac{T_c - T_s}{R_s}, \tag{11}$$

$$0 = \frac{T_c - T_s}{R_s} - \frac{T_s - T_a}{R_a} - \frac{p_s - p_a}{Z_a}, \text{ and} \tag{12}$$

$$0 = \frac{p_c - p_s}{Z_s} - \frac{p_s - p_a}{Z_a}. \tag{13}$$

As in regions II and III, these are combined with Eq. (10), which ensures that $T_c = 310$ K. The circuit diagram for this region is shown in Fig. 4. The constants used in region I are given in Table 3.

c. Regions IV and V: Naked

Recall that in region III, the human chooses its clothing thickness so as to maintain its core temperature. In conditions that are too hot and humid, we will be unable to find a physical solution in region III. This occurs because the core cannot be maintained at 310 K even with clothing of zero thickness, that is, with $R_f = Z_f = 0$. In such hot and humid conditions, the ideal human chooses to be naked ($\phi = 0$) as designed by Steadman (1979), and the blood flow to the skin is increased so as to reduce R_s and Z_s as needed. In region IV, the conservation Eqs. (1)–(7) simplify to (Steadman 1979)

$$0 = Q - Q_v - \frac{T_c - T_s}{R_s}, \tag{14}$$

$$0 = \frac{T_c - T_s}{R_s} - \frac{T_s - T_a}{R_a} - \frac{p_s - p_a}{Z_a}, \text{ and} \tag{15}$$

$$p_s = \frac{Z_a p_c + Z_s p_a}{Z_a + Z_s}. \tag{16a}$$

To ensure a healthy human, these are combined with Eq. (10) as before. The circuit diagram for region IV is shown in Fig. 5. For sufficiently hot and humid conditions, this solution becomes unphysical because p_s exceeds the saturation vapor pressure of sweat $\phi_{\text{salt}} p^*(T_s)$, and the standard heat index becomes undefined; see the undefined region in Table 2 of Steadman (1979). To extend the heat index into region V, we let sweat drip off the skin, which replaces the mass-balance Eq. (16a) with

$$p_s = \phi_{\text{salt}} p^*(T_s). \tag{16b}$$

The circuit diagram for region V is shown in Fig. 6. In summary, the conservation equations for regions IV and V are (14), (15), and

$$p_s = \min \left[\frac{Z_a p_c + Z_s p_a}{Z_a + Z_s}, \phi_{\text{salt}} p^*(T_s) \right]. \tag{16}$$

The constants used in regions IV and V are given in Table 4.

d. Region VI: Warming

In conditions that are too hot and humid, we will be unable to find a physical solution in region V. This occurs because the core cannot be maintained at 310 K even when the circulatory system has driven the skin temperature to that of the core, making $R_s = Z_s = 0$. In such hot and humid conditions, it is necessary to reduce the metabolic rate Q to maintain $T_c = 310$ K; thus, Q becomes the free variable. In the limit of $R_s = Z_s = 0$, Eqs. (14)–(16) simplify to

$$0 = Q - Q_v - \frac{T_c - T_a}{R_a} - \frac{p_c - p_a}{Z_a}. \tag{17}$$

The circuit diagram for region VI is shown in Fig. 7. The constants used in region VI are given in Table 5.

TABLE 2. Variables and constants for regions II and III.

| Variable | Value | Interpretation |
|---------------------------|---|---|
| R_f | Variable | Resistance to heat transfer through the clothing |
| T_c | 310 K | Core temperature |
| p_c | $\phi_{\text{salt}} p^*(T_c)$ | Core vapor pressure |
| ϕ | 0.84 | Fraction of skin covered by clothing (Steadman 1979) |
| R_s | $0.0387 \text{ m}^2 \text{ K W}^{-1}$ | Resistance to heat transfer through the skin (Steadman 1979) |
| Z_s | $52.1 \text{ m}^2 \text{ Pa W}^{-1}$ | Resistance to water transfer through the skin (Steadman 1979) |
| Z_f | rR_f | Resistance to water transfer through the clothing (Steadman 1979) |
| r | 124 Pa K^{-1} | Ratio of Z_f and R_f (Steadman 1979) |
| R_a | $[\phi_{\text{rad}} \epsilon \sigma (T_s^2 + T_a^2)(T_s + T_a) + h_c]^{-1}$ | Resistance to heat transfer through the boundary layer of air in contact with exposed skin |
| Z_a | $(60.6 \text{ Pa K}^{-1})/h_c$ | Resistance to water transfer through the boundary layer of air in contact with exposed skin (Steadman 1979) |
| h_c | $17.4 \text{ W K}^{-1} \text{ m}^{-2}$ | Heat transfer coefficient between surface of exposed skin and air (Steadman 1979) |
| ϕ_{rad} | 0.85 | Effective fraction of exposed skin exchanging longwave radiation with air (or surfaces with temperature T_a) (Steadman 1979) |
| ϵ | 0.97 | Longwave emissivity of exposed skin (Steadman 1979) |
| \bar{R}_a | $[\bar{\phi}_{\text{rad}} \bar{\epsilon} \sigma (T_f^2 + T_a^2)(T_f + T_a) + \bar{h}_c]^{-1}$ | Resistance to heat transfer through the boundary layer of air in contact with clothing |
| \bar{Z}_a | $(60.6 \text{ Pa K}^{-1})/\bar{h}_c$ | Resistance to water transfer through the boundary layer of air in contact with clothing (Steadman 1979) |
| \bar{h}_c | $11.6 \text{ W K}^{-1} \text{ m}^{-2}$ | Heat transfer coefficient between exterior of clothing and air (Steadman 1979) |
| $\bar{\phi}_{\text{rad}}$ | 0.79 | Effective fraction of clothing exchanging longwave radiation with air (or surfaces with temperature T_a) (Steadman 1979) |
| $\bar{\epsilon}$ | 0.97 | Longwave emissivity of clothing (Steadman 1979) |

In regions I–V, Q is chosen to be equal to 180 W m^{-2} of skin surface, consistent with a person walking outdoors at 1.4 m s^{-1} , or about 3 mi h^{-1} (Steadman 1979). There are several ways to think about the reduction in Q that is required in region VI. Near the cool edge of region VI, we may think of this reduction in Q as a behavioral choice to reduce the walking pace. This has its limits, however, as even a resting metabolic rate is 51.8 W m^{-2} (Parsons 2014). Another way to think about the reduction in Q is as a conscious choice to directly cool the core, for example, by drinking ice water or through some actively powered cooling system. If none of these behavioral choices are available, then a third way to think about region VI is to dispense with the steady-state assumption and recognize that there will be a positive dT_c/dt . In this case, Q is

pegged to the constant value of 180 W m^{-2} and dT_c/dt becomes the free variable through a modified version of Eq. (17), namely,

$$C_c \frac{dT_c}{dt} = Q - Q_v - \frac{T_c - T_a}{R_a} - \frac{p_c - p_a}{Z_a}. \quad (18)$$

Since this is no longer a steady-state equation, there is no simple and analogous circuit diagram. The constants used in region VI with Eq. (18) are given in Table 6.

e. Summary of the derivations

Here, we summarize the preceding derivations. Recall that R_f is proportional to the clothing thickness and R_s is inversely

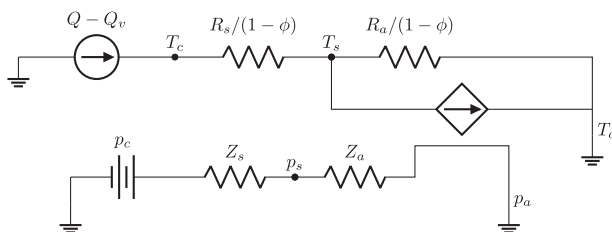


FIG. 4. Diagram illustrating the potentials and resistances for sensible heat transfer (top circuit) and water transfer (bottom circuit) for region I. In region I, a constant T_c is maintained by varying ϕ between 1 and 0.84, which is the threshold value for region II.

related to the skin blood flow. We refer to Steadman's clothed solutions (with variable clothing thickness and constant skin blood flow) as region III and Steadman's naked solutions (with variable skin blood flow) as region IV. The transition from region III to IV happens at a heat index of about 298 K, at which the clothing thickness becomes zero. Moving from region III into colder temperatures, the existing heat index becomes undefined because Steadman assumes a fixed reference vapor pressure of 1.6 kPa, which would exceed the saturation pressure at an air temperature less than $p^{*-1}(1.6 \text{ kPa}) = 287 \text{ K}$, where p^{*-1} is the inverse function of the saturation vapor pressure given by Eq. (9). To extend the heat index to cold regimes, we define a region II where the clothing thickness is still variable, but the reference vapor pressure is set to the heat index's saturation vapor pressure rather than 1.6 kPa. The transition from region III to II thus occurs at a heat index of 287 K. At sufficiently low air temperatures, the clothing thickness becomes infinite, indicating that the clothing (which covers only 84% of the skin) becomes so thick as to be perfectly insulating; we define this as the boundary between regions II and I, at which the heat index is about 238 K. In region I, we hold the clothing thickness fixed at infinity and let the clothed skin fraction vary; in this region, the heat index is defined as the temperature of saturated air that would solve the equations with the same clothed fraction. In region I, the heat index is very nearly equal to the air temperature, regardless of the relative humidity.

Moving from region IV into hotter temperatures, the existing heat index becomes undefined because Steadman equates the skin's evaporation rate to the sweating rate. When the air temperature is sufficiently high, this causes the skin's vapor pressure to exceed its saturation value. By allowing sweat to drip off the skin, we are able to extend the definition of the heat index into higher-temperature regimes. To do so, we define a region V where the skin blood flow is still variable, but the skin's vapor pressure is equal to its saturation vapor pressure. To accommodate this new constraint in region V, we remove the mass-conservation equation for the skin's water budget; physically, this allows excess water to drip off the sweat-soaked skin. Note that the transition from region IV to V occurs when Eqs. (16a) and (16b) give the same skin vapor pressure, and this does not correspond to a single heat index, but a range of heat indices from 308 to 333 K. For sufficiently hot and humid conditions, the skin blood flow becomes

infinite, making the temperature of the skin equal to that of the core. We call this the boundary between regions V and VI, which occurs at a heat index of 345 K.¹ In region VI, it is impossible to maintain a healthy core temperature without a reduction in the metabolic rate Q , a new source of internal cooling, or growth in the core temperature. The heat index is then defined as the temperature (at the reference vapor pressure of 1.6 kPa) that would give the same variable Q with $dT_c/dt = 0$ or, equivalently, the temperature at the reference vapor pressure that would give the same dT_c/dt with the reference Q . Sample values of the extended heat index in regions IV–VI are shown in Fig. 8.

f. Comparisons with the polynomial fit

For compatibility with Steadman's heat index, we use all of the same parameter values, except that we replace some of Steadman's linearized equations with the full T^4 dependence for longwave radiation, a formal expression of ventilation cooling [Eq. (8)], and a more accurate formula for saturation vapor pressure of water (or of ice, when the temperature is below freezing) [Eq. (9)]. These improvements, which are necessary at very high temperatures, cause deviations from the original heat index of less than 1 K throughout regions III and IV where the original heat index is defined, ensuring backward compatibility. This can be verified from the right panel of Fig. 9, which shows the difference between Steadman's heat index [taken directly from Table 2 of Steadman (1979)] and the heat index computed using our formalism, sampled over $293 \leq T_a \leq 323 \text{ K}$ with increments of 1 K and $0 \leq \text{RH} \leq 1$ with increments of 0.1. In Fig. 9, pairs of temperature and humidity for which Steadman's heat index was not defined [including the value in parentheses in Table 2 of Steadman (1979)] are excluded. For comparison, an oft-used polynomial fit (Rothfus 1990) has errors with respect to Steadman's original heat index as large as 7 K (see the left panel of Fig. 9). Even with the National Weather Service's adjustments to the polynomial fit [National Weather Service (2014), replicated in appendix B], the polynomial fit still has errors as large as 2 K in comparison with Steadman's published values (see the middle panel).

Furthermore, the National Weather Service (NWS) uses its polynomial fit not just to interpolate the heat index values given by Steadman, but also to extrapolate them into the undefined regions, that is, into what we refer to here as regions V and VI. The top panel of Fig. 10 replicates the "heat index chart" displayed on the NWS website (National Weather Service 2022a), which displays the polynomial fit in degrees Fahrenheit. In the original chart, the four colors, from yellow to red, are labeled by the NWS with "caution," "extreme caution," "danger," and "extreme danger." The middle panel of Fig. 10 shows the errors in that chart, as compared with the extended heat index calculated here. We see that the NWS values are

¹ To hundredths of a degree, the heat index values separating regions I–VI are 238.49, 287.16, 298.44, a range from 308.23 to 333.39, and 344.65 K, respectively. Although the heat index can be calculated to this precision or higher, we will henceforth report the heat index as an integer value.

TABLE 3. Variables and constants for region I.

| Variable | Value | Interpretation |
|---------------------|---|---|
| ϕ | Variable | Fraction of skin that is clothed |
| T_c | 310 K | Core temperature |
| p_c | $\phi_{\text{salt}} p^*(T_c)$ | Core vapor pressure |
| R_s | $0.0387 \text{ m}^2 \text{ K W}^{-1}$ | Resistance to heat transfer through the skin (Steadman 1979) |
| Z_s | $52.1 \text{ m}^2 \text{ Pa W}^{-1}$ | Resistance to water transfer through the skin (Steadman 1979) |
| R_a | $[\phi_{\text{rad}} \epsilon \sigma (T_s^2 + T_a^2)(T_s + T_a) + h_c]^{-1}$ | Resistance to heat transfer through the boundary layer of air in contact with the exposed skin |
| Z_a | $(60.6 \text{ Pa K}^{-1})/h_c$ | Resistance to water transfer through the boundary layer of air in contact with the exposed skin (Steadman 1979) |
| h_c | $17.4 \text{ W K}^{-1} \text{ m}^{-2}$ | Heat transfer coefficient between surface of exposed skin and air (Steadman 1979) |
| ϕ_{rad} | 0.85 | Effective fraction of exposed skin exchanging longwave radiation with air (or surfaces with temperature T_a) (Steadman 1979) |
| ϵ | 0.97 | Longwave emissivity of exposed skin (Steadman 1979) |

negatively biased (biased low) by as much as 28°F (16 K). Therefore, studies relying on this extrapolation will have underestimated the risk of high heat. The bottom panel of Fig. 10 displays a corrected version of the NWS chart using the same numerical boundaries between the four colors. Since 161°F (345 K) is the heat index that separates regions V and VI, we learn that the edge of the labeled region in this NWS chart corresponds closely to the boundary between regions V and VI; that is, the unlabeled region is where ill effects are unavoidable even for an ideal human under ideal circumstances. In another NWS chart, polynomial extrapolation is used well into region VI (National Weather Service 2022b).

3. Physical interpretation of the heat index

By construction, each value of the heat index maps to a unique value of a physical variable. In region I, that variable is ϕ , which describes the fraction of the body that must be fully insulated to maintain a core temperature of 310 K. In regions II and III, the variable is R_f , which describes the thickness of clothing required (over 84% of the body) to keep the core temperature at 310 K; R_f is proportional to the clothing thickness d via (Steadman 1979)

$$R_f = (16.7 \text{ m K W}^{-1})d. \quad (19)$$

In regions IV and V, the variable is R_s , which describes the skin blood flow required to keep the core at 310 K; the relation between R_s and the skin blood flow \dot{V} is (Gagge et al. 1972)

$$\frac{1}{R_s} = \frac{1}{R_{s0}} + \rho c \dot{V}/A, \quad (20)$$

where $R_{s0} = 0.189 \text{ m}^2 \text{ K W}^{-1}$ is the heat transfer resistance of the tissue, $\rho = 1000 \text{ kg m}^{-3}$ is the density of blood,

$c = 4184 \text{ J kg}^{-1} \text{ K}^{-1}$ is the specific heat capacity of blood, and A is the skin area as given in Table 1. In region VI, the variable is dT_c/dt , which describes how quickly the core temperature is rising above its ideal value of 310 K.

The first three rows of Fig. 11 plot the clothing fraction, clothing thickness, and skin blood flow as functions of the heat index in regions I–V. At the hot end of region V, the blood flow is so high that it pegs the skin temperature to that of the core. At this point, the cooling effects of perspiration and blood flow have been maxed out. In region VI, it is not possible to maintain a healthy core temperature of 310 K with the walking metabolic rate of 180 W m^{-2} , and so dT_c/dt is positive. While unhealthy, a positive dT_c/dt is not necessarily fatal for a young, healthy adult if the core temperature equilibrates below the critical thermal maximum of 315 K, which is commonly used as the threshold for heat death (Ferris et al. 1938; Bouchama and Knochel 2002). As shown in the next subsection, the equilibrated T_c is a function only of the heat index, as opposed to a more general function of air temperature and humidity. As shown in the fourth row of Fig. 11, the equilibrium core temperature enters the range for heat exhaustion, heat stroke, and heat death ($T_c > 310, 313,$ and 315 K) (Bouchama and Knochel 2002) at heat indices of 345, 357, and 366 K, respectively.² For a sustained heat index above 366 K, it is not a question of whether a fatal core temperature will be reached, but how soon it will be reached. As also shown in the next subsection, the time it takes T_c to rise from 310 to 315 K is also a function only of the heat index; this duration is plotted in the fifth row of Fig. 11. Many studies have used a wet-bulb temperature of 35°C

² More precise values are 344.65, 357.42, and 366.44 K, respectively.

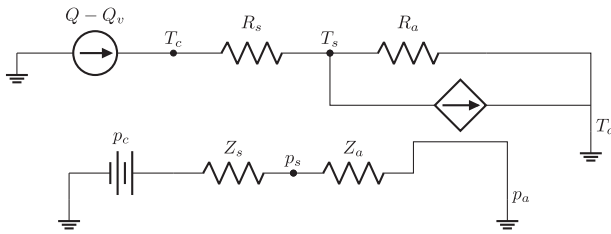


FIG. 5. Diagram illustrating the potentials and resistances for sensible heat transfer (top circuit) and water transfer (bottom circuit) in region IV, one of the two original cases of Steadman (1979).

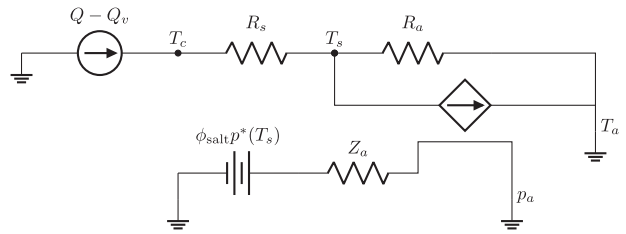


FIG. 6. Diagram illustrating the potentials and resistances for sensible heat transfer (top circuit) and water transfer (bottom circuit) in region V.

as a threshold value that is fatal to humans (Sherwood and Huber 2010; Pal and Eltahir 2016; Frieling et al. 2017; Raymond et al. 2020). In reality, each heat index corresponds to a range of wet-bulb temperatures: the fatal heat index of 366 K corresponds to wet-bulb temperatures from 32° to 38°C.

Functions of the heat index in region VI

Here, we show that, in region VI, the equilibrium core temperature \tilde{T}_c and the time τ it takes the core to get to the critical thermal maximum of 315 K are functions only of the heat

index. Previous work has shown that the polynomial extrapolated heat index is highly correlated to the equilibrium core temperature (Santee and Wallace 2005). With the analytic extension of the heat index as done in this paper, the relation is made exact.

We start with Eq. (18), which can be written as

$$f(T_c, T_a, p_a) \equiv C_c \frac{dT_c}{dt} \tag{21}$$

$$= Q - \eta Q \left\{ c_{pa}(T_c - T_a) + \frac{L\hat{R}_a}{\hat{R}_v p} [\phi_{\text{salt}} p^*(T_c) - p_a] \right\} - \phi_{\text{rad}} \epsilon \sigma (T_c^4 - T_a^4) - h_c (T_c - T_a) - \frac{\phi_{\text{salt}} p^*(T_c) - p_a}{Z_a} \tag{22}$$

$$= Q - \underbrace{\eta Q c_{pa} T_c - \eta Q \frac{L\hat{R}_a}{\hat{R}_v p} \phi_{\text{salt}} p^*(T_c) - \phi_{\text{rad}} \epsilon \sigma T_c^4 - h_c T_c - \frac{\phi_{\text{salt}} p^*(T_c)}{Z_a}}_{g(T_c)} + \underbrace{\eta Q c_{pa} T_a + \phi_{\text{rad}} \epsilon \sigma T_a^4 + h_c T_a}_{h(T_a)} + \underbrace{\eta Q \frac{L\hat{R}_a}{\hat{R}_v p} p_a + \frac{p_a}{Z_a}}_{k(p_a)} \tag{23}$$

$$= g(T_c) + h(T_a) + k(p_a). \tag{24}$$

TABLE 4. Variables and constants for regions IV and V.

| Variable | Value | Interpretation |
|---------------------|---|---|
| R_s | Variable | Resistance to heat transfer through the skin |
| T_c | 310 K | Core temperature |
| p_c | $\phi_{\text{salt}} p^*(T_c)$ | Core vapor pressure |
| Z_s | $(6.0 \times 10^8 \text{ Pa W}^4 \text{ m}^{-8} \text{ K}^{-5}) R_s^5$ | Resistance to water transfer through the skin (Steadman 1979) |
| R_a | $[\phi_{\text{rad}} \epsilon \sigma (T_s^2 + T_a^2)(T_s + T_a) + h_c]^{-1}$ | Resistance to heat transfer through the boundary layer of air in contact with the exposed skin |
| Z_a | $(60.6 \text{ Pa K}^{-1})/h_c$ | Resistance to water transfer through the boundary layer of air in contact with the exposed skin (Steadman 1979) |
| h_c | $12.3 \text{ W K}^{-1} \text{ m}^{-2}$ | Heat transfer coefficient between surface of exposed skin and air (Steadman 1979) |
| ϕ_{rad} | 0.80 | Effective fraction of exposed skin exchanging longwave radiation with air (or surfaces with temperature T_a) (Steadman 1979) |
| ϵ | 0.97 | Longwave emissivity of exposed skin (Steadman 1979) |

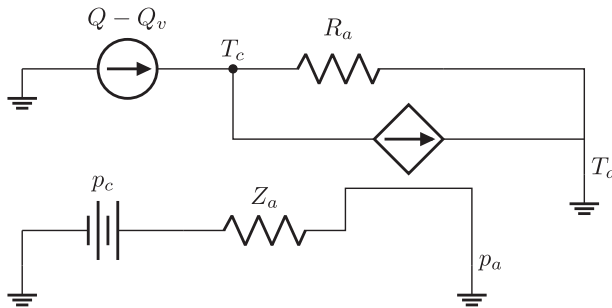


FIG. 7. Diagram illustrating the potentials and resistances for sensible heat transfer (top circuit) and mass transfer (bottom circuit) in region VI. In this region, to maintain $T_c = 310$ K, Q has to be varied.

We see that dT_c/dt is equal to the sum of three functions, each of which depends only on T_c , T_a , and p_a , respectively. Now, consider a given T_a and p_a . For the purposes of the derivation here, let us define $T_{c0} = 310$ K and denote the heat index by T . By the definition of the heat index in region VI,

$$f(T_{c0}, T_a, p_a) = f(T_{c0}, T, p_{a0}),$$

which implies that

$$g(T_{c0}) + h(T_a) + k(p_a) = g(T_{c0}) + h(T) + k(p_{a0}).$$

Adding $g(T_c) - g(T_{c0})$ to both sides, we get

$$f(T_c, T_a, p_a) = f(T_c, T, p_{a0}), \tag{25}$$

which holds for arbitrary T_c . Next, by definition, the equilibrium core temperature \tilde{T}_c satisfies $f(\tilde{T}_c, T_a, p_a) = 0$, so using Eq. (25), we can write this as $f(\tilde{T}_c, T, p_{a0}) = 0$, which can be solved for \tilde{T}_c in terms of T . In other words, \tilde{T}_c is a function only of the heat index T , as opposed to having some other functional dependence on T_a and p_a . Similarly, let us define

τ to be the time it takes the core to increase in temperature from $T_{c0} = 310$ K to the critical thermal maximum of $T_{c1} = 315$ K. By rearrangement of Eq. (21), we can write this as

$$\tau = \int_{T_{c0}}^{T_{c1}} \frac{C_c dT_c}{f(T_c, T_a, p_a)} \tag{26}$$

$$= \int_{T_{c0}}^{T_{c1}} \frac{C_c dT_c}{f(T_c, T, p_{a0})}, \tag{27}$$

where we have used Eq. (25) in the last line. Therefore, τ is a function only of the heat index T .

4. Validity of the ideal-human assumption

Steadman’s model is idealized in many ways: it assumes that the human is doing no heavy labor, has unrestricted access to drinking water, has a perfect system of thermal regulation, and has no modesty (disrobing as needed to maximize thermal comfort). Since the heat index is constructed from a best-case scenario—a perfect human responding in an ideal way—it serves as a robust lower bound on the physiological consequences of high heat and humidity. In our extension of the heat index, we maintain this “best-case scenario” approach by imposing no limits on the skin blood flow or sweat rate. As shown in the next two subsections, imposing realistic bounds on the skin blood flow and sweat rate changes the apparent temperature by no more than a few kelvins.

Similarly, the ambient condition of the Steadman model is also idealized: it assumes the human is under the shade with a constant breeze. When the human stays under the sunlight with a lower wind speed, the body can be warmed up significantly, depending on the amount of shortwave radiation absorbed and the amount of reduced evaporation rate. Therefore, 366 K can be considered a conservative upper bound on the heat index that can be survived with sustained exposure.

TABLE 5. Variables and constants for region VI using Eq. (17).

| Variable | Value | Interpretation |
|---------------------|---|---|
| Q | Variable | Metabolic rate |
| T_c | 310 K | Core temperature |
| p_c | $\phi_{\text{salt}} p^*(T_c)$ | Core vapor pressure |
| R_a | $[\phi_{\text{rad}} \epsilon \sigma (T_c^2 + T_a^2)(T_c + T_a) + h_c]^{-1}$ | Resistance to heat transfer through the boundary layer of air in contact with skin |
| Z_a | $(60.6 \text{ Pa K}^{-1})/h_c$ | Resistance to water transfer through the boundary layer of air in contact with the skin (Steadman 1979) |
| h_c | $12.3 \text{ W K}^{-1} \text{ m}^{-2}$ | Heat transfer coefficient between surface of exposed skin and air (Steadman 1979) |
| ϕ_{rad} | 0.80 | Effective fraction of exposed skin exchanging longwave radiation with air (or surfaces with temperature T_a) (Steadman 1979) |
| ϵ | 0.97 | Longwave emissivity of exposed skin (Steadman 1979) |

TABLE 6. Variables and constants for region VI using Eq. (18).

| Variable | Value | Interpretation |
|---------------------|---|---|
| dT_c/dt | variable | Tendency of core temperature |
| T_c | 310 K | Initial core temperature |
| C_c | $M_c c_{pc}/A$ | Heat capacity of the core per skin area |
| p_c | $\phi_{\text{salt}} p^*(T_c)$ | Core vapor pressure |
| R_a | $[\phi_{\text{rad}} \epsilon \sigma (T_c^2 + T_a^2)(T_c + T_a) + h_c]^{-1}$ | Resistance to heat transfer through the boundary layer of air in contact with the skin |
| Z_a | $(60.6 \text{ Pa K}^{-1})/h_c$ | Resistance to water transfer through the boundary layer of air in contact with the skin (Steadman 1979) |
| h_c | $12.3 \text{ W K}^{-1} \text{ m}^{-2}$ | Heat transfer coefficient between surface of exposed skin and air (Steadman 1979) |
| ϕ_{rad} | 0.80 | Effective fraction of exposed skin exchanging longwave radiation with air (or surfaces with temperature T_a) (Steadman 1979) |
| ϵ | 0.97 | Longwave emissivity of exposed skin (Steadman 1979) |

In reality, with a diverse population in diverse circumstances, the fatality rate will climb to unacceptable levels well before the heat index reaches such a value.

a. Finite skin blood flow

In the model of thermoregulation, we assume that the skin blood flow can be made as large as needed, all the way up to infinite flow (equivalently, $R_s = 0$). In reality, the largest skin blood flow recorded in the literature is 7.8 L min^{-1} (Rowell 1974; Simmons et al. 2011), which, using Eq. (20), corresponds to $R_s = 0.004 \text{ m}^2 \text{ K W}^{-1}$. Although our extension of Steadman’s model has intentionally maintained its ideal nature, we could have imposed this upper bound on the skin blood flow and defined the extended heat index accordingly. This would make the hot boundary of region V retreat to lower temperatures, albeit subtly as shown in Fig. 12. From Eq. (14), a nonzero R_s implies that there must exist a finite

temperature difference between the core and the skin, and so in region VI, Eq. (18) is replaced with

$$C_c \frac{dT_c}{dt} = Q - Q_v - \frac{T_c - T_s}{R_s} \quad \text{and} \quad (28)$$

$$0 = \frac{T_c - T_s}{R_s} - \frac{T_s - T_a}{R_a} - \frac{\phi_{\text{salt}} p^*(T_s) - p_a}{Z_a}, \quad (29)$$

where R_s is fixed at $0.004 \text{ m}^2 \text{ K W}^{-1}$. We can solve the two equations for dT_c/dt , and the heat index is defined as the air temperature T_a that would give the same dT_c/dt at $p_a = p_{a0}$. With the modification, the heat index changes, but by less than 2 K, and with changes approaching 2 K only at the otherworldly conditions of saturated air at a temperature of 360 K (87°C, or 188°F) (see Fig. 12). Therefore, we conclude that using infinite skin blood flow does not make a significant difference relative to using a realistic bounded skin blood flow.

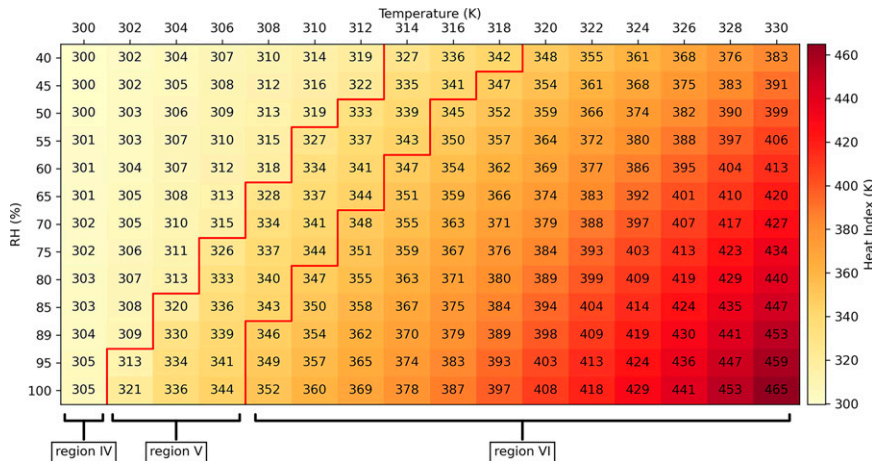


FIG. 8. The heat index as a function of the air temperature and relative humidity. Red lines separate regions IV, V, and VI. The heat index was previously undefined in regions I and II (not shown here) and in regions V and VI.

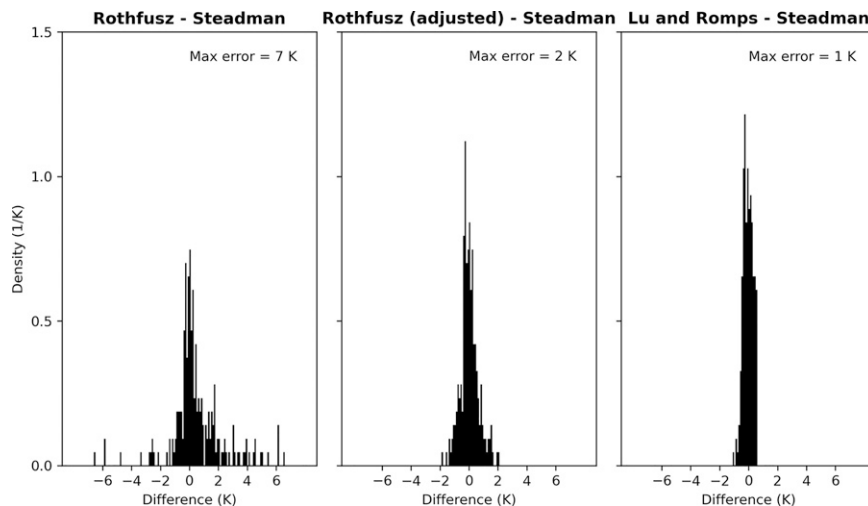


FIG. 9. The differences between Steadman's heat index and (left) the polynomial fit of Rothfusz (1990), (center) the Rothfusz polynomial fit with adjustments (National Weather Service 2014), and (right) our extended heat index. Steadman's heat index is taken directly from Table 2 of Steadman (1979), omitting the undefined heat index (including the value given there in parentheses).

b. Finite sweat rate

Steadman's human model also assumes that the sweat rate can reach any desired value to keep the body cool. However, a human has a maximum sweat rate of about $2\text{--}4\text{ L h}^{-1}$ (Mack and Nadel 2011). We can check, however, if the model would ever require a sweat rate higher than this limit. Using the mass transfer term $(p_s - p_a)/Z_a$ in each region, we can plot contours of the sweat rate on temperature–humidity space. Referring to Fig. 13, we see that the maximum sweat rate occurs at around $T_a = 360\text{ K}$ and $\text{RH} = 0$ and has the value of 3.3 L h^{-1} . Therefore, only in this extreme circumstance does the model generate a sweat rate that is in the vicinity of the documented maximum of $2\text{--}4\text{ L h}^{-1}$. Note that the negative sweat rate in other circumstances means that the environmental vapor condenses onto the skin, releasing latent heat to the human body. In these situations, sweat is unable to cool the body since the ambient vapor pressure is higher than that at the skin.

5. Change in the heat index in warming scenarios

For the summertime at the ARM SGP site with a previously undefined heat index (due to high temperature and humidity) as shown in Fig. 1, we can now calculate the heat index and its distribution, which is shown in Fig. 14. Note that the transition from region IV to the previously undefined region V occurs at heat indices from 308 to 333 K, and this range is thus shaded in gray color with gradient. In the current climate from year 2012 to 2021, inclusive, the maximum heat index in the summertime is right around the boundary of region V, where the body has maximized its capacity for evaporative cooling, with excess sweat dripping off the skin.

To illustrate the change in the heat index under different warming scenarios, two other distributions are plotted by adding either 5 (blue) or 10 (dark blue) K to the SGP summertime temperatures while keeping the relative humidities fixed. The change in the heat index is not a simple translation as the distribution in temperature–humidity space (see Fig. 1) but has a nonlinear response to warming. In region V, the only thermoregulatory mechanism left to the body is to crank up the skin blood flow, altering the temperature of its skin, which is, in practice, limited to a range of only a few kelvins. Therefore, this adaptation is exhausted within only a few kelvins of warming, throwing the body into region VI. As a consequence, warming the SGP air temperatures by 10 K increases the maximum heat index by 40 K. In this scenario, 12% of the time has a heat index above 345 K, which guarantees heat exhaustion: even for an ideal human at rest in the shade with ample water, their core temperature would be forced to rise above 310 K.

6. Conclusions

We have extended the definition of the heat index so that it applies to a much wider range of temperature and humidity, while retaining backward compatibility. As in Steadman's original definition, the underlying model of thermoregulation represents a human with optimal physiology (e.g., unlimited rates of sweating and skin blood flow) and behavior (e.g., seeking shade and disrobing as needed). Each heat index value corresponds to a unique physiological state that specifies the clothing fraction, clothing thickness, skin blood flow rate, and the rate of change in the core temperature. In physiological states for which the time derivative of the core temperature is positive, that rate can be mapped to an equilibrium core

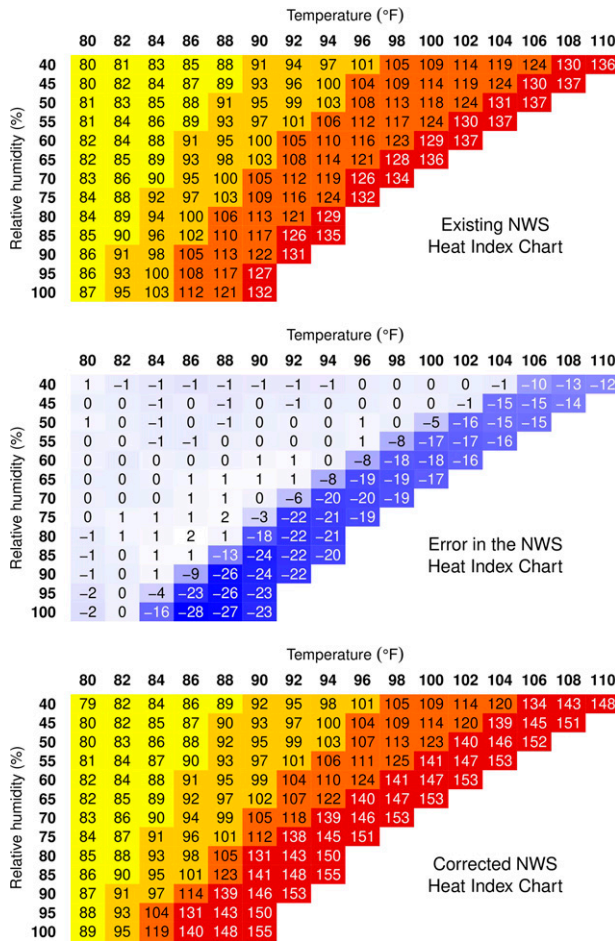


FIG. 10. (top) The heat index chart displayed on the website of the National Weather Service (NWS) with values in degrees Fahrenheit (National Weather Service 2022a). (middle) The errors in that chart, defined by subtracting the extended heat index. (bottom) The corrected version of the NWS chart.

temperature or the time needed to reach the fatal core temperature.

The correspondence between the heat index and the physiological state allows us to assess future habitability under different warming scenarios. Even for a very fit individual (approaching the optimal human being assumed in the thermoregulation model), the rate at which a human can expel heat is still constrained by physical laws that govern, for example, heat conduction and the evaporation of water. In a sufficiently hot and humid environment, the human body runs out of tricks for regulating its core temperature, leading to sickness or death.

Both the original heat index and the extended heat index presented here are constructed from a model of a human with optimal physiology and behavior. Therefore, a suitable interpretation of the heat index is that it approximates the apparent temperature for a young, healthy adult. In this regard, the mapping given here from heat index to physiological response (e.g., exhaustion, stroke, or death) should be considered

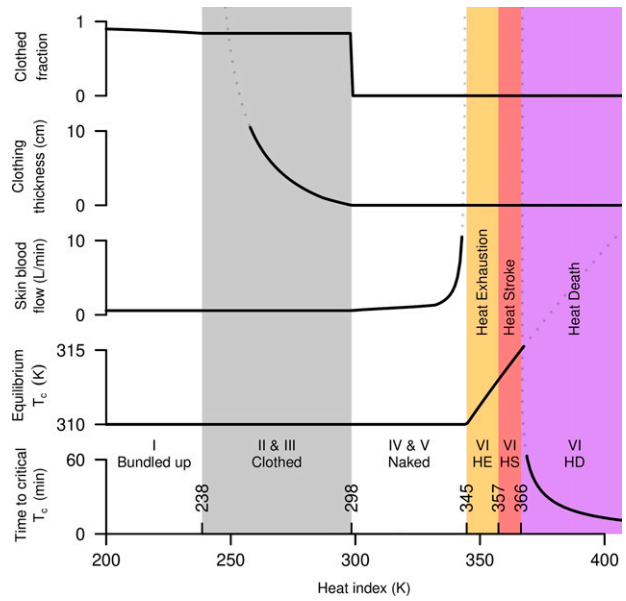


FIG. 11. The human condition as a function of the heat index.

a best-case scenario that serves as a lower bound on the health effects for any real individual. It should be anticipated that heat index values below the nominally fatal value of 366 K may be fatal for a large fraction, if not a majority, of the population.

Acknowledgments. This work was supported by the U.S. Department of Energy’s Atmospheric System Research program through the Office of Science’s Biological and Environmental Research program under Contract DE-AC02-05CH11231. Observational data were obtained from the Atmospheric Radiation Measurement (ARM) user facility, a U.S. Department of Energy (DOE) Office of Science user facility managed by the Biological and Environmental research program.

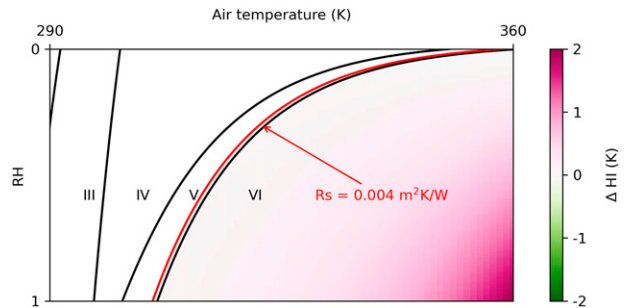


FIG. 12. Change in the heat index if we set an upper bound of 7.8 L min^{-1} ($R_s = 0.004 \text{ m}^2 \text{ K W}^{-1}$) on the skin blood flow. The black curves separate the extended heat index regions with unbounded skin blood flow. Note that the rightmost black curve separating regions V and VI is the constant $R_s = 0$ curve. The red curve is the constant $R_s = 0.004 \text{ m}^2 \text{ K W}^{-1}$ curve, corresponding to a skin blood flow of 7.8 L min^{-1} . The color scale shows the change in the heat index, which only reaches as high as 2 K for saturated air of a temperature of 360 K (87°C , or 188°F).

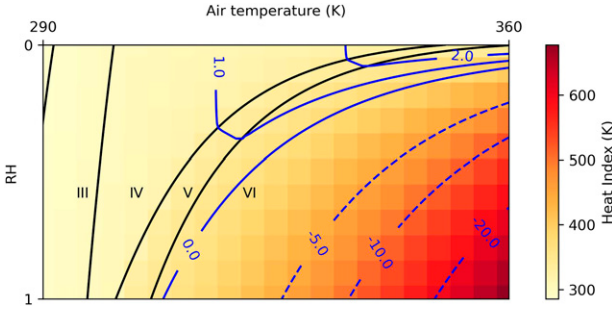


FIG. 13. The blue contours show the sweat rate of the human model with units of liters per hour. Negative values represent condensation rates of the ambient vapor onto the skin. Black curves separate the regions of the heat index as defined before. The color scale shows the value of the heat index within $0 \leq T_a \leq 360$ K and $0 \leq RH \leq 1$.

Data availability statement. The DOE ARM data are available online (<https://www.arm.gov/capabilities/observatories/sgp>).

APPENDIX A

Numerical Solutions in Regions I–VI

To solve the algebraic equations presented in the paper, the following procedures are used.

a. Numerical solution in regions II and III

We use Eqs. (1)–(7) to solve for R_f as follows. First, use Eq. (5) to solve for p_s ,

$$p_s = \frac{Z_a p_c + Z_s p_a}{Z_a + Z_s}.$$

Substituting into Eq. (2) and noting that R_a has a nonlinear dependence on T_s (see Table 2), we can solve Eq. (2) for T_s using a root solver. We then solve for \bar{T}_s using Eq. (1). The remaining unknowns are p_f , T_f , \bar{p}_s , and R_f . Using Eq. (4), we can write R_f in terms of T_f as

$$R_f = \bar{R}_a \frac{\bar{T}_s - T_f}{T_f - T_a}.$$

We can use Eqs. (6) and (7) to write \bar{p}_s and p_f in terms of R_f as

$$\bar{p}_s = \frac{(\bar{Z}_a + rR_f)p_c + Z_s p_a}{\bar{Z}_a + rR_f + Z_s} \quad \text{and} \quad (\text{A1})$$

$$p_f = \frac{\bar{Z}_a p_c + (rR_f + Z_s)p_a}{\bar{Z}_a + rR_f + Z_s}. \quad (\text{A2})$$

Substituting the expression for R_f into these last two equations, we now have R_f , \bar{p}_s , and p_f as functions of T_f . Substituting all three of these expressions into Eq. (3), we can solve for T_f using a root solver. That then gives us R_f , \bar{p}_s , and p_f .

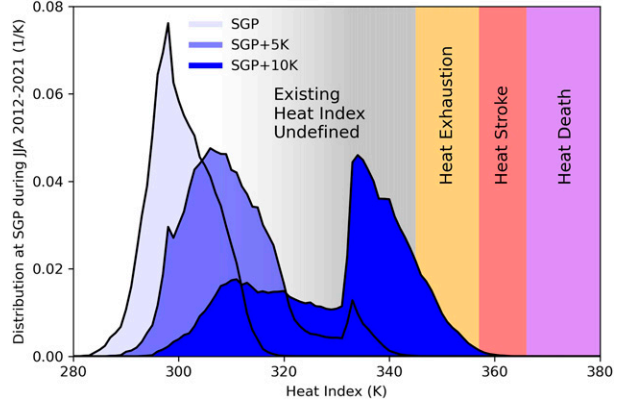


FIG. 14. Distribution of the heat index at the ARM SGP site from 1-min measurements of temperature and humidity during JJA 2012–21 (light blue) and the same but adding 5 (medium blue) and 10 (dark blue) K to the temperatures while keeping the relative humidities unchanged. The gray region with gradient shows the range of heat indices where region IV makes a transition to region V. (The transition occurs within a finite range of heat index from 308 to 333 K and therefore is represented by the gray color with gradient.)

b. Numerical solution in region I

We can solve Eqs. (11)–(13) for ϕ as follows. First, use Eq. (13) to solve for p_s ,

$$p_s = \frac{Z_a p_c + Z_s p_a}{Z_a + Z_s}.$$

Substituting into Eq. (12), we get

$$0 = \frac{T_c - T_s}{R_s} - \frac{T_s - T_a}{R_a} - \frac{p_c - p_a}{Z_a + Z_s}. \quad (\text{A3})$$

Since R_a depends on T_s , this must be solved for T_s using a root solver. Once T_s is obtained in this way, ϕ can be obtained from Eq. (11) as

$$\phi = 1 - R_s \frac{Q - Q_v}{T_c - T_s}.$$

We define the heat index as the T_a that gives the same ϕ for $p_a = \min[p_{a0}, p^*(T_a)]$, which, since $p^*(T_a)$ is always less than p_{a0} in region I, is simply $p^*(T_a)$. This is calculated by using a root solver to find the T_a that gives, using the procedure above, the correct ϕ .

c. Numerical solution in regions IV and V

We can solve Eqs. (14)–(16) for R_s as follows. First, we solve Eq. (14) for T_s , which gives T_s as a function of R_s ,

$$T_s = T_c - (Q - Q_v)R_s.$$

Plugging this into Eq. (16), and noting that Z_s is a function of R_s , we get p_s as an explicit function of R_s . Therefore, we can write all the terms of Eq. (15) as explicit functions of R_s , for which we can then find using a root solver. We then define the heat index as the T_a that gives the same R_s for

$p_a = p_{a0}$ at $T_c = 310$ K. This is calculated by using a root solver to find the T_a that gives, using the procedure above, the correct R_s .

d. Numerical solution in region VI

Given T_a and p_a , Eq. (17) provides an explicit expression for dT_c/dt . We then define the heat index as the T_a that gives the same dT_c/dt for $p_a = p_{a0}$. Since R_a depends nonlinearly on T_a , Eq. (17) is solved for this T_a using a root solver.

APPENDIX B

Text of National Weather Service (2014)

This appendix reproduces the content of the website that gives the polynomial fit used by the NWS for calculating the heat index (National Weather Service 2014). The website was described as last modified on 28 May 2014 when it was accessed on 16 February 2022. The document to which it refers is Rothfusz (1990). The content has been lightly edited to present the equations in American Meteorological Society journal mathematical style.

The computation of the heat index is a refinement of a result obtained by multiple regression analysis carried out by Lans P. Rothfusz and described in a 1990 National Weather Service (NWS) Technical Attachment (SR 90-23). The regression equation of Rothfusz is

$$\begin{aligned} \text{HI} = & -42.379 + 2.049\ 015\ 23T + 10.143\ 331\ 27\text{RH} \\ & - 0.224\ 755\ 41\text{TRH} - 0.006\ 837\ 83T^2 \\ & - 0.054\ 817\ 17\text{RH}^2 + 0.001\ 228\ 74T^2\text{RH} \\ & + 0.000\ 852\ 82\text{TRH}^2 - 0.000\ 001\ 99T^2\text{RH}^2, \end{aligned}$$

where T is temperature in degrees Fahrenheit and RH is relative humidity in percent. HI is the heat index expressed as an apparent temperature in degrees Fahrenheit. If the RH is less than 13% and the temperature is between 80 and 112 degrees Fahrenheit, then the following adjustment is subtracted from HI:

$$\text{ADJUSTMENT} = \frac{13 - \text{RH}}{4} \sqrt{\frac{17 - |T - 95|}{17}}.$$

On the other hand, if the RH is greater than 85% and the temperature is between 80 and 87 degrees Fahrenheit, then the following adjustment is added to HI:

$$\text{ADJUSTMENT} = \frac{\text{RH} - 85}{10} \frac{87 - T}{5}.$$

The Rothfusz regression is not appropriate when conditions of temperature and humidity warrant a heat index value below about 80 degrees Fahrenheit. In those cases, a simpler formula is applied to calculate values consistent with Steadman's results:

$$\text{HI} = 0.5[T + 61.0 + 1.2(T - 68.0) + 0.094\text{RH}].$$

In practice, the simple formula is computed first and the result averaged with the temperature. If this heat index value is 80 degrees Fahrenheit or higher, the full regression equation along with any adjustment as described above is applied.

The Rothfusz regression is not valid for extreme temperature and relative humidity conditions beyond the range of data considered by Steadman.

REFERENCES

- Amnuaylojaroen, T., A. Limsakul, S. Kirtsang, N. Parasin, and V. Surapipith, 2022: Effect of the near-future climate change under RCP8.5 on the heat stress and associated work performance in Thailand. *Atmosphere*, **13**, 325, <https://doi.org/10.3390/atmos13020325>.
- Anderson, G. B., M. L. Bell, and R. D. Peng, 2013: Methods to calculate the heat index as an exposure metric in environmental health research. *Environ. Health Perspect.*, **121**, 1111–1119, <https://doi.org/10.1289/ehp.1206273>.
- Bouchama, A., and J. P. Knochel, 2002: Heat stroke. *N. Engl. J. Med.*, **346**, 1978–1988, <https://doi.org/10.1056/NEJMra011089>.
- Buettner, K. J. K., 1959: Diffusion of liquid water through human skin. *J. Appl. Physiol.*, **14**, 261–268, <https://doi.org/10.1152/jap.1959.14.2.261>.
- Dahl, K., R. Licker, J. T. Abatzoglou, and J. Delect-Barreto, 2019: Increased frequency of and population exposure to extreme heat index days in the United States during the 21st century. *Environ. Res. Commun.*, **1**, 075002, <https://doi.org/10.1088/2515-7620/ab27cf>.
- Delworth, T. L., J. D. Mahlman, and T. R. Knutson, 1999: Changes in heat index associated with CO₂-induced global warming. *Climatic Change*, **43**, 369–386, <https://doi.org/10.1023/a:1005463917086>.
- Diem, J. E., C. E. Stauber, and R. Rothenberg, 2017: Heat in the southeastern United States: Characteristics, trends, and potential health impact. *PLOS ONE*, **12**, e0177937, <https://doi.org/10.1371/journal.pone.0177937>.
- Diffenbaugh, N. S., J. S. Pal, F. Giorgi, and X. Gao, 2007: Heat stress intensification in the Mediterranean climate change hotspot. *Geophys. Res. Lett.*, **34**, L11706, <https://doi.org/10.1029/2007GL030000>.
- Fanger, P. O., 1970: *Thermal Comfort: Analysis and Applications in Environmental Engineering*. Danish Technical Press, 244 pp.
- Ferris, E. B., M. A. Blankenhorn, H. W. Robinson, and G. E. Cullen, 1938: Heat stroke: Clinical and chemical observations on 44 cases. *J. Clin. Invest.*, **17**, 249–262, <https://doi.org/10.1172/JCI100949>.
- Frieling, J., and Coauthors, 2017: Extreme warmth and heat-stressed plankton in the tropics during the Paleocene-Eocene thermal maximum. *Sci. Adv.*, **3**, e1600891, <https://doi.org/10.1126/sciadv.1600891>.
- Fryar, C. D., D. Kruszon-Moran, Q. Gu, and C. Ogden, 2018: Mean body weight, height, waist circumference, and body mass index among adults: United States, 1999–2000 through 2015–2016. CDC National Health Statistics Rep. 122, 16 pp., <https://www.cdc.gov/nchs/data/nhsr/nhsr122-508.pdf>.
- Gagge, A., J. A. J. Stolwijk, and Y. Nishi, 1972: An effective temperature scale based on a simple model of human physiological regulatory response. *ASHRAE Trans.*, **7**, 247–262.
- Mack, G. W., and E. R. Nadel, 2011: Body fluid balance during heat stress in humans. *Comprehensive Physiology*, R. Terjung, Ed., American Physiological Society, 187–214, <https://doi.org/10.1002/cphy.cp040110>.
- Mather, J. H., and J. W. Voyles, 2013: The ARM Climate Research Facility: A review of structure and capabilities. *Bull. Amer.*

- Meteor. Soc.*, **94**, 377–392, <https://doi.org/10.1175/BAMS-D-11-00218.1>.
- Modarres, R., M. Ghadami, S. Naderi, and M. Naderi, 2018: Future heat stress arising from climate change on Iran's population health. *Int. J. Biometeor.*, **62**, 1275–1281, <https://doi.org/10.1007/s00484-018-1532-4>.
- National Weather Service, 2014: The heat index equation. Accessed 16 February 2022, https://www.wpc.ncep.noaa.gov/html/heatindex_equation.shtml.
- , 2022a: Heat index chart. Accessed 16 February 2022, <https://www.weather.gov/safety/heat-index>.
- , 2022b: Heat index chart. Accessed 16 February 2022, <https://www.weather.gov/jetstream/hi>.
- Newburgh, L. H., Ed., 1949: *Physiology of Heat Regulation and the Science of Clothing*. WB Saunders, 457 pp.
- Opitz-Stapleton, S., L. Sabbag, K. Hawley, P. Tran, L. Hoang, and P. H. Nguyen, 2016: Heat index trends and climate change implications for occupational heat exposure in Da Nang, Vietnam. *Climate Serv.*, **2–3**, 41–51, <https://doi.org/10.1016/j.cliser.2016.08.001>.
- Pal, J. S., and E. A. B. Eltahir, 2016: Future temperature in south-west Asia projected to exceed a threshold for human adaptability. *Nat. Climate Change*, **6**, 197–200, <https://doi.org/10.1038/nclimate2833>.
- Parsons, K., 2014: *Human Thermal Environments: The Effects of Hot, Moderate, and Cold Environments on Human Health, Comfort, and Performance*. CRC Press, 560 pp.
- Rahman, M. B., R. Salam, A. R. Md. Towfiqul Islam, A. Tasnuva, U. Haque, S. Shahid, Z. Hu, and J. Mallick, 2021: Appraising the historical and projected spatiotemporal changes in the heat index in Bangladesh. *Theor. Appl. Climatol.*, **146**, 125–138, <https://doi.org/10.1007/s00704-021-03705-x>.
- Rao, K. K., and Coauthors, 2020: Projections of heat stress and associated work performance over India in response to global warming. *Sci. Rep.*, **10**, 16675, <https://doi.org/10.1038/s41598-020-73245-3>.
- Raymond, C., T. Matthews, and R. M. Horton, 2020: The emergence of heat and humidity too severe for human tolerance. *Sci. Adv.*, **6**, eaaw1838, <https://doi.org/10.1126/sciadv.aaw1838>.
- Romps, D. M., 2017: Exact expression for the lifting condensation level. *J. Atmos. Sci.*, **74**, 3891–3900, <https://doi.org/10.1175/JAS-D-17-0102.1>.
- Rothfus, L. P., 1990: The heat index “equation” (or, more than you ever wanted to know about heat index). NWS Southern Region Headquarters Tech. Attachment SR 90-23, 2 pp., https://www.weather.gov/media/ffc/ta_htindx.PDF.
- Rowell, L. B., 1974: Human cardiovascular adjustments to exercise and thermal stress. *Physiol. Rev.*, **54**, 75–159, <https://doi.org/10.1152/physrev.1974.54.1.75>.
- Santee, W. R., and R. F. Wallace, 2005: Comparison of weather service heat indices using a thermal model. *J. Therm. Biol.*, **30**, 65–72, <https://doi.org/10.1016/j.jtherbio.2004.07.003>.
- Sherwood, S. C., and M. Huber, 2010: An adaptability limit to climate change due to heat stress. *Proc. Natl. Acad. Sci. USA*, **107**, 9552–9555, <https://doi.org/10.1073/pnas.0913352107>.
- Simmons, G. H., B. J. Wong, L. A. Holowatz, and W. L. Kenney, 2011: Changes in the control of skin blood flow with exercise training: Where do cutaneous vascular adaptations fit in? *Exp. Physiol.*, **96**, 822–828, <https://doi.org/10.1113/expphysiol.2010.056176>.
- Steadman, R. G., 1979: The assessment of sultriness. Part I: A temperature-humidity index based on human physiology and clothing science. *J. Appl. Meteor.*, **18**, 861–873, [https://doi.org/10.1175/1520-0450\(1979\)018<0861:TAOSPI>2.0.CO;2](https://doi.org/10.1175/1520-0450(1979)018<0861:TAOSPI>2.0.CO;2).